
Article:
Rigby, S.E., Fay, S.D., Clarke, S.D. et al. (5 more authors) (2016) Measuring spatial pressure distribution from explosives buried in dry Leighton Buzzard sand. International Journal of Impact Engineering, 96. pp. 89-104. ISSN 0734-743X

https://doi.org/10.1016/j.ijimpeng.2016.05.004

Measuring Spatial Pressure Distribution from Explosives Buried in Dry Leighton Buzzard Sand

S.E. Rigby[a,*], S.D. Fay[a,b], S.D. Clarke[a], A. Tyas[a,b], J.J. Reay[b], J.A. Warren[a,b], M. Gant[c], I. Elgy[c]

[a] *Department of Civil & Structural Engineering, University of Sheffield, Mappin Street, Sheffield, S1 3JD, UK*
[b] *Blastech Ltd., The BioIncubator, 40 Leavygreave Road, Sheffield, S3 7RD, UK*
[c] *Defence Science and Technology Laboratory (Dstl), Porton Down, Salisbury, Wiltshire, SP4 0JQ, UK.*

Abstract

Direct measurement of the intense loading produced by the detonation of a buried explosive is an extremely difficult task. Historically, high-fidelity measurement techniques have not been sufficiently robust to capture the extremely high pressures associated with such events, and researchers have relied on 'global' measurements such as the average loading acting over a particular area of interest. Recently, a large-scale experimental approach to the direct measurement of the spatial and temporal variation in loading resulting from an explosive event has been developed, which utilises Hopkinson pressure bars (HPBs) inserted through holes in a large target plate such that their faces lie flush with the loaded face. This article presents results from ten experiments conducted at 1/4 scale, using 17 HPBs to measure the spatial pressure distribution from explosives buried in dry Leighton Buzzard sand, a commonly available sand used in many geotechnical applications. Localised pressure measurements are used in conjunction with high speed video to provide a detailed examination of the physical processes occurring at the loaded face, as well allowing quantification of these effects. Example pressure-time and impulse-time traces are provided in full to allow researchers to use this data for validation of numerical modelling approaches.

Keywords: Buried explosive, Experiment, High speed video, Hopkinson pressure bar, Pressure measurement

1. Introduction

Shallow-buried improvised explosive devices (IEDs) are a common threat in conflict zones across the world. As a result of the additional confinement provided by the surrounding soil the effects of the explosive are focussed and channelled vertically, causing a large amplification in energetic output directly above a detonated subsurface IED. This intense loading can cause significant damage to and potentially breach the undersides of military and civilian vehicles, exposing its occupants to lethal pressures. If the hull armour remains intact, the momentum

*Tel.: +44 (0) 114 222 5724

imparted to the vehicle from the combined effects of blast pressure and soil throw may still be significant enough to cause life-threatening injuries such as brain damage and spinal cord compression associated with rapid global acceleration, or traumatic amputation associated with rapid localised acceleration from deformation of the vehicle underside [1].

Whilst the underlying physical processes involved with buried explosive events are reasonably well reported in the literature, the process by which the load is imparted to the target, as well as the exact form of the applied load, has not yet been definitively characterised. Furthermore, the understanding of the role of soil properties in such events is still in its infancy. Understanding the interaction of the effects of an IED and a target structure is of utmost importance, as this dictates whether protective systems are capable of resisting a specific threat, or whether its occupants remain at risk. Accordingly, we must fully investigate this process before we can safely design and assess vehicle platforms and infrastructure which may be subjected to improvised explosive attacks.

The current authors have recently developed a large-scale experimental approach to the direct measurement of the spatial and temporal variation in loading resulting from an explosive event [2]. Whilst previous work (detailed in the following section) has utilised a similar approach, the work presented herein is the first of this type at a larger scale. The testing apparatus utilises Hopkinson pressure bars (HPBs) [3], inserted through holes situated within a large, effectively rigid target plate, such that their faces lie flush with the loaded face of the plate. The ends of each HPB will therefore be subjected to the reflected blast pressure acting at a discrete point on the plane of the target face. An array of these HPBs can be used to provide spatially and temporally resolved information on the imparted load, and can record pressures of up to ~500 MPa. This paper presents results from two series of 1/4 scale experiments conducted using high explosive charges buried within a well controlled soil mass. 17 HPBs in total are used within a radius of 100 mm from the target centre. The results are used in combination with high speed video stills to investigate and characterise the loading mechanisms present at the target face. Compiled results are presented in detail to offer well-controlled experimental data for validation of numerical modelling approaches.

2. A review of buried explosion events

2.1. Physical processes of a buried explosion

Bergeron et al. provide a thorough review of the physical processes which occur immediately following detonation of a buried explosive [4]. This comprises three distinct phases, which are summarised here.

- *Phase 1 – Detonation and early interaction with the soil*

  After detonation is initiated in a high explosive material, a detonation wave travels outwards away from the point of detonation. This extremely high pressure detonation wave initiates a chemical reaction in the explosive, resulting in a sudden release of energy as the explosive rapidly converts into a dense gas at temperatures in excess of 6,000°C and pressures in excess of 20 GPa [5]. Once this wave reaches the edge of the explosive, it is mostly transmitted in to the surrounding soil skeleton due to similar acoustic impedances of the two materials. This causes localised crushing of the soil immediately adjacent to the explosive, with zones of permanent plastic deformation, and zones of recoverable elastic deformation further out from the explosive. The exact sizes of these regions are very much dependent on soil properties and geometry of the event, and dictate the amount of energy lost to irrecoverable work and hence the energy available to impart work to the target. Parameters which influence this include: depth of burial; explosive size/shape; physical soil properties such as density, strength and cohesion; and moisture content/air voids ratio.

- *Phase 2 – Gas expansion*

  When the compressive wave reaches the soil surface, a large acoustic impedance mismatch at the soil/air interface results in a small portion of the wave being transmitted in to the air as a pre-cursor shock, with the remainder being transmitted back through the soil as a tensile wave. This tensile wave, combined with the vertical force exerted to the soil from the high pressure detonation products causes a soil cap to be ejected from the surface of the soil at supersonic velocity. Initially, this soil 'bubble' continues to confine the still-expanding detonation products, which impart an extremely high momentum to the soil and acts as a piston to sustain and drive the pre-cursor air shock. As the detonation products continue to expand volumetrically, the soil bubble will thin and at some point rupture and vent the detonation products to the surrounding air.

- *Phase 3 – Soil ejecta*

  The soil cap which is ejected in the early stages of the explosion has a relatively small volume. In the later stages, the high pressure detonation products continue to do work to the surrounding medium and continue to shear the region of soil adjacent to the detonation products. This results in long-term ejection of a large volume of soil, over durations several orders of magnitude longer than Phase 2. It is generally accepted that Phase 2 and 3 above produce markedly different loading conditions when interacting with a target situated some distance above the soil surface. The loading during Phase 2 is typically highly localised, short duration

and high magnitude, and is caused by combined impingement of the ejected soil plug and high pressure detonation products on the target face. Phase 3 loading is typically more evenly distributed across the target face and is caused by momentum transfer from the gradually excavated late-time soil ejecta [5]. An inverse cone of ejected material, with an included angle between 60° and 90°, describes the post-event crater [4].

2.2. Research into buried explosions

The topic of buried explosions has received much attention over recent years. It is not the authors' intention to provide the reader with a comprehensive review of all related research; this review will serve to provide the reader with all necessary background information to the current study and to highlight notable contributions to the field.

The subject of quantification of the effect of buried explosions on above ground structures began to gather interest in North America in the 1970s and 1980s [6, 7]. Westine et al. [8] used an 'impulse plug' technique to measure the output from a buried explosive at discrete points on a target surface. Here, small, rigid plugs of known mass were inserted into holes within a larger reflecting boundary located above the surface in which an explosive was buried. The velocity of each plug was measured and the specific impulse acting at the plug location was calculated. An empirical approach was developed from the test data, which was extended by Tremblay [9] to calculate the total impulse acting on a variety of target geometries.

Bergeron et al. [4] conducted a comprehensive experimental investigation of the detonation of 100 g C4 buried within a soil, employing various diagnostics including air and soil mounted pressure transducers, flash x-ray radiography and high speed photography, and post-test crater measurements. Hlady [10] conducted experiments using two soil types with different particle size distributions (PSDs); a coarse-grained sand and a fine-grained silty-clay. 25 g C4 charges were detonated beneath a target of known mass which was permitted to translate vertically. A linear voltage displacement transducer was used to measure the rise-height of the moving mass and hence deduce total impulse acting on the target face. Various parameters such as moisture content, burial depth, and stand-off (distance from soil surface to target) were investigated, however the results are hampered by lack of control of the soil conditions and demonstrate considerable spread. Nevertheless, a significant increase was seen in the output from an explosive buried in wet soil compared to the output from an explosive buried in dry soil. The trials also highlighted the existence of an optimal burial depth: with no overburden there is no soil present to focus the blast, with a large overburden the soil is able to contain most of the explosive energy, hence the optimal burial depth lies between these two extremes.

Grujicic et al. developed an improved compaction model for sand for use in transient non-linear dynamics explicit simulation software [11]. This was then used to investigate the loading mechanism from land mines buried in sand with differing moisture contents [5]. It was observed that dry sands and wet sands produce markedly different loading conditions, i.e. dry sands produce more ‘blast-type‘ loading, whereas wet sands produce more ‘bubble-type’ loading. These are caused by rupture of the soil bubble and venting of the detonation products in dry soils, and impact of the driven soil bubble in saturated soils. These mechanisms have since been experimentally confirmed by the current authors [12]. Similar numerical studies have since been conducted, e.g. [13, 14, 15], yet the ability to rigorously validate numerical modelling remains inhibited by the lack of well-controlled experimental data.

In order to circumvent the difficulties associated with preparing large soil samples required for full-scale testing, some researchers have conducted ‘laboratory-scale’ tests using no more than a few grams of explosive, e.g. the work of Fox et al. on the global momentum transferred to rigid targets [16, 17], and the work of Fourney et al. [18] on spatial distribution of buried loading. Here, the distribution of loading was studied using two techniques: firstly by using steel plates with different diameters and the same mass to investigate global impulse output; and secondly by using free-flying steel plugs embedded within a larger target to study local impulse. These tests showed that the output from explosives buried in saturated soil can be up to twice the impulse from explosives buried in a dry soil.

2.3. Previous work at the University of Maryland

Researchers at the Dynamics Effects Laboratory at the University of Maryland, USA, have conducted a large number of small-scale experiments on quantifying the distribution of loading from buried explosive events [19, 20, 21, 22, 23]. The tests used Detasheet charges with explosive masses between 0.8–16 g in order for the researchers to be able to conduct a large number of tests at a reasonable cost. The standard set up was using 4.4 g at an approximate scale of 1/10 compared to STANAG threat level M2 [24], with data recorded using either a single array of HPBs at different radial offsets, or a circle of HPBs at the same radial offset. High speed video was also used as a diagnostic; either by filming the soil bubble expansion in free air, or filming the soil bubble impacting a clear, rigid, PMMA sheet from above. Dry and saturated sand was investigated (as well as water, although this was predominantly for code validation purposes), but little information was given with regards to the preparation of the soil bed and how a uniform test bed was achieved, making it difficult to distinguish between the variability of the testing procedure and the variability of the event itself.

The results showed that the peak pressures measured for the saturated sand were consistently higher than those for the dry sand. On the contrary, the specific impulse was seen to be higher for the dry sand directly above the charge, which fell to below the values for the saturated sand further from the target centre. Interestingly the highest peak pressures for the saturated sand were recorded slightly away from the target centre, often outside of the radius of the charge, rather than above the charge as may be expected [21]. Two main loading phases were identified from the pressure traces: early-time loading resulting from momentum transfer from the high velocity soil directly above the charge impacting the target; and late-time loading by impact of an annular jet of material excavated from the crater [19]. These phases loosely correspond to Phase 2 and Phase 3 loading introduced by Bergeron [4] and detailed in section 2.1 above. The results offer valuable data and insights into buried explosive loading, however, the soil material when scaled up to its full-sized equivalent will have a particle size in the order of 10 mm. This could lead to directionality effects, particularly given the shallow depth of burial used in the testing. In the absence (prior to the present study) of any detailed spatial and temporal loading data at larger scale, the significance of this effect is unclear.

While the general mechanisms of buried explosions are fairly well-known, and indeed some important trends have been shown, the major area for research is that of understanding which of these mechanisms contribute the majority of the loading, and hence also the provision of accurate spatially and temporally resolved data for numerical modelling purposes. There is currently a lack of well controlled experimental data in the literature, particularly at large-scale. The authors aim to address this with the current testing methodology.

3. Experimental work

3.1. Justification for 1/4 length scale testing

The full-scale version of STANAG threat level M2, as given in the Allied Engineering Publication *Procedures for evaluating the protection level of logistic and light armoured vehicles (AEP-55)* [24], specifies the use of a 6 kg TNT explosive mass, or a 5 kg PE4 mass assuming a TNT equivalence of 1.2 [25]. Small scale buried explosive tests are inexpensive and easy to prepare, however this must be balanced with the requirement for tight control over the conditions of the geotechnical test bed, in particular the material situated above the charge. Furthermore, it becomes difficult to stably detonate high explosives below ~50 g mass. At 1/4 length scale, the full-scale burial depth of 100 mm scales to 25 mm and the full scale charge mass of 5 kg scales to 78 g. This is seen as

a fair compromise between the benefits of small-scale testing and the need for geometrical conditions that scale accurately.

Generally the geotechnical material is not scaled when testing buried explosives at smaller scales. This means that, at quarter scale, the soil particles are four times larger than would be used if the soil was also scaled according to the length scale of the test. Previous testing by the current authors has shown no difference between the output from explosives buried in soil whose scaled-up particle sizes were two and four times greater than their full scale equivalent [26]. We can assume that this extends to soil whose scaled-up particle size is equal to the full scale test, and therefore we can be reasonably confident that it is valid to model 1/4 scale events using full-sized soil. With this in mind, by comparing the data presented from the current study with existing data collected at smaller scale, we are able to make comments on the validity of testing buried explosive events at laboratory scale.

3.2. Apparatus

The experimental apparatus developed by Clarke et al. [2] is housed at the University of Sheffield Blast & Impact Lab. in Buxton, Derbyshire, UK. At the 1/4 length scale used in the current testing, the threat comprises a 78 g PE4 charge formed into a cylinder with a diameter:height ratio of 3:1 and a diameter of 57.1 mm. The charge was situated within a 3 mm thick PVC container which was open at the top. The detonators were inserted through the base of the explosive, as this was found to remove spurious data associated with fragment strike and electrical noise from the breakwire [27]. Although designed for buried explosive events, the experimental apparatus has also been used to measure free-air blast effects [28, 29].

A cylindrical steel container, with 500 mm internal diameter, 375 mm height and 30 mm wall thickness was filled with the soil to be used in testing, and the explosive was buried to a depth of 28 mm, measured from the soil surface to the top of the charge. Here, an additional 3 mm burial depth is provided in addition to the 25 mm mandated in AEP-55 to account for the missing PVC cap. The soil container was located with the soil surface at distances of 105 mm and 140 mm beneath the underside of the target plate and aligned such that the centre of the container sat directly beneath the centre of the target plate. The geometry of the test arrangement can be seen in Figure 1.

The 100 mm thick, 1400 mm diameter steel target plate was mounted on four load cells which were fixed to an effectively rigid steel fibre and bar reinforced concrete dual ‘goalpost’ frame, Figure 2(a–b). A 10.5 mm diameter hole was drilled through the centre of the plate, with subsequent holes drilled at 25 mm spacing in perpendicular

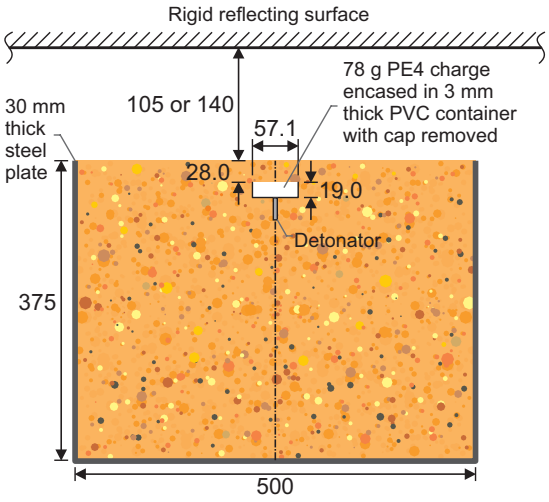

Figure 1: Geometry of test arrangement (length dimensions in mm)

arrays either side of the central hole, as in Figure 2(c). These arrays are termed the $-x$, $+x$, $-y$ and $+y$ arrays according to the coordinate axes in Figure 2(d). Through each hole, 10 mm diameter, 3.25 m long EN24(T) steel HPBs were inserted and suspended from a receiver frame placed atop the main reaction frame. The holes through which the HPBs were inserted were purposefully oversized to avoid any coupling effects between the plate and HPBs. The HPBs and support frame were earthed to prevent ionisation from the detonation products producing spurious electrical noise.

Kyowa KSP-2-120-E4 semi-conductor strain gauges were mounted in pairs on the perimeter of each HPB, 250 mm from the loaded face, in a Wheatstone-bridge circuit to ensure that only the axial strain component was recorded. From the axial strain, the pressure acting on the loaded face can be deduced. A total of 17 bars were used in this test series, with one central bar and four radial bars situated in each array at 25, 50, 75 and 100 mm radial offset from the plate centre, r. Previous testing by Fourney et al. has shown that a single array is not adequate to capture the complex non-coaxial breakout of the expanding soil bubble [20].

Strain data were recorded using 14-Bit digital oscilloscopes at a sample rate of 1.56 MHz, triggered via a voltage drop in a breakwire embedded in the detonator to synchronise the recordings with the detonation. The oscilloscopes have isolated inputs to reduce cross-talk between signals. Signal conditioning and amplification were combined in a differential circuit which is particularly beneficial in circuits where the signal of interest is small in comparison to large voltage offsets or noise. The HPBs are capable of recording loading durations of

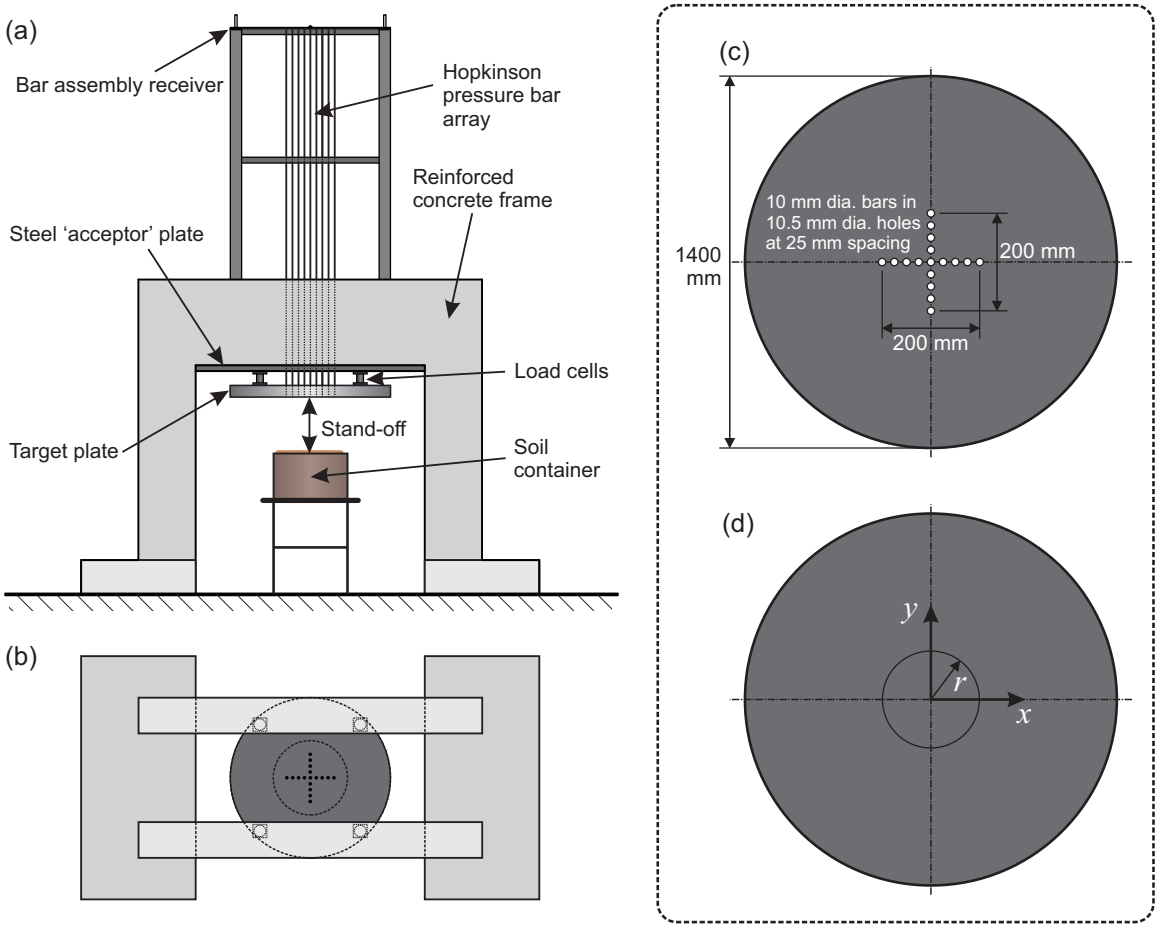

Figure 2: Schematic of the testing apparatus [not to scale]: (a) elevation; (b) plan; (c) bar arrangement used in the current test series; (d) coordinate axes

~1.2 ms before reflection of the signal from the distal end of the bar interferes with the incoming pressure pulse. Hence, this arrangement is focussed only on Phase 2 type loading (section 2.1). The load cells on which the plate are mounted can be used to record the total load acting on the target plate, inclusive of Phase 3 loading, however the primary focus of this paper is the early stages of loading. Preliminary numerical modelling work indicated that Phase 3 loading contributes very little to the dynamic deflection of deformable targets subjected to buried explosions [2], hence the main focus of research should be in quantifying Phase 2 loading.

A Photron SA-Z high speed video (HSV) camera with a 105 mm Nikon lens was housed within a protective structure and used to film each test. The events were filmed at a resolution of 1024×184 at a rate of 100,000 fps and 1/400,000 s exposure time, with an aperture of f/2.8 using two halogen lights to achieve the desired illumination. The camera was positioned level height with the soil surface and its field-of-view included the entire diameter of the soil container to enable late-time (Phase 3) effects to be seen, as well as the early stages of loading. The camera was triggered via a separate breakwire embedded in the detonator, enabling the images to be synchronised with HPB data. HSV stills are used in this article to act as a diagnostic to aid interpretation of the HPB signals.

3.3. Soil preparation and test plan

Ten tests were conducted using Leighton Buzzard (LB), a commonly available sand used in many laboratory applications. A grading of 14/25 was chosen for this test series, giving a range of particle sizes between 0.6–1.18 mm (a relatively uniform particle size distribution, see Figure 3(a)). LB sand is a rounded to well-rounded quartz silica sand, see Figure 3(b). With silica being the dominant material, LB has a specific gravity, G_s, of 2.65.

A moisture content of 2.5% was specified for all tests. The moisture content, w, is given as

$$w(\%) = M_w/M_s \times 100 \tag{1}$$

where M_w is the mass of water and M_s is the dry mass of solids. A constant dry density, ρ_d, of 1.60 Mg/m^3 was specified for all tests, giving the soil bed a required compaction bulk density, ρ, of 1.64 Mg/m^3, where

$$\rho = \rho_d(1 + w) \tag{2}$$

The soil is therefore relatively dry with a saturation ratio, S_r, of 10%, given as

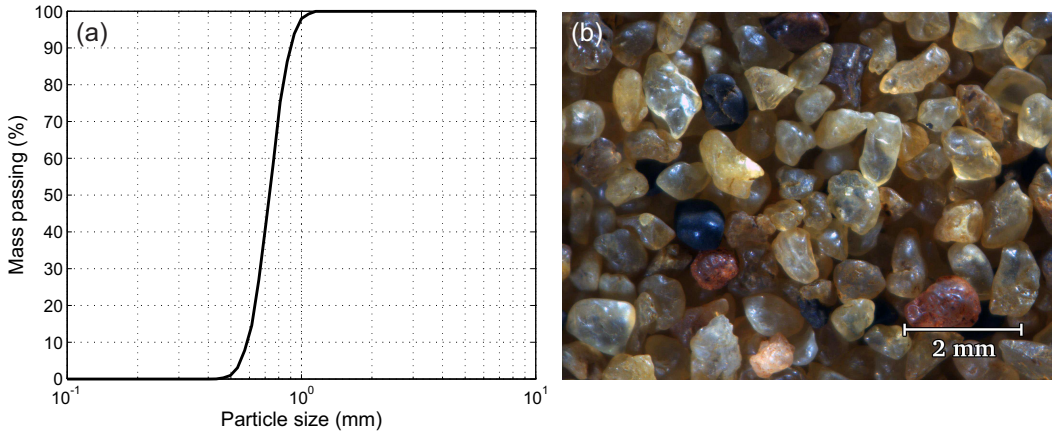

Figure 3: (a) Particle size distribution, (b) optical microscope image of Leighton Buzzard sand [30]

$$S_r(\%) = \frac{w\rho_d}{(1 - \rho_d/G_s)} \tag{3}$$

The LB is weighed as it enters a forced action mixer, and the correct mass of sand and water required for three tests is added. Mixing typically takes five minutes, but will continue until the water is evenly distributed. A sample is then taken from the mixer and the moisture content is checked. If this is within tolerance, the mass and moisture content are recorded and the first lift may begin.

Approximately 60 kg of material is poured into the steel container for the first lift. A timber plywood board is placed on the sand surface, Figure 4(a), and the sand height is recorded and checked. A stiffened steel compaction tool, Figure 4(b), is placed on top of the plywood board and mechanically struck until the sand surface reaches the required height for the specified bulk density. Measurements of the final sand level are recorded and the plywood board and compaction tool are removed from the container. The un-compacted height of the second lift will exceed the height of the steel container, so a laterally restrained 150 mm deep, 500 mm internal diameter steel collar, Figure 4(c), is seated on the top lip of the container. A further 60 kg of LB is emptied into the container, which is then levelled and compacted as per the first lift. After the plywood board, compaction tool and and collar are removed, a small amount of LB (<1 kg) should be left protruding from the soil container. This excess material is tamped into the soil bed with a steel screeding tool. The soil surface is then marked for charge placement, Figure 4(d). The process is repeated for an additional two containers until all the soil in the forced action mixture

has been emptied. A polythene sheet seals each soil container so that no moisture is lost during storage. This sheet is removed immediately before the charge is buried and the firing sequence begins and the container remains uncovered for no longer than 15 minutes.

Figure 4: Images of soil preparation equipment: (a) timber plywood board (b) stiffened steel compaction tool (c) steel collar (d) soil container filled with LB being marked for charge placement

The detonator, break wire and charge are configured prior to placement in the soil container, Figure 5(a) and (b). A 100 mm deep, slotted plastic shutter which is 5 mm greater in diameter than the charge is aligned with the centre of the soil bed, Figure 5(c). Sand is removed from within the shutter as it is pressed into the soil. When the shutter top is flush with the sand surface, excavation is complete. A flat steel bar is used to place a hole at the base of the excavation for the detonator command line and breakwire umbilical. An inclined channel is prepared from the base of the shutter to the edge of the container. The charge and umbilical can now be buried, Figure 5(d) and checked for depth and lateral alignment, Figure 5(e). The excavated material is weighed, Figure 5(f), and placed in a sealed bag in order to backfill to the correct density and moisture content. The shutter can then be removed and the cable umbilical secured to the container wall. The overburden is then carefully placed above the charge, Figure 5(g), and the soil surface is made good with a screeding level and is ready for firing, Figure 5(h).

By using the methodology for preparation of the soil bed described above, the density of the geotechnical material can be achieved to within ± 0.2 Mg/m^3 of the target density, and the moisture content can be achieved to within $\pm 0.05\%$ of the target in terms of moisture content [31, 32]. All geometrical variables were kept constant for the two test series with the exception of stand-off: five tests were conducted with 140 mm distance from the soil surface to the target, and five tests were conducted with 105 mm. The test plan is summarised in Table 1.

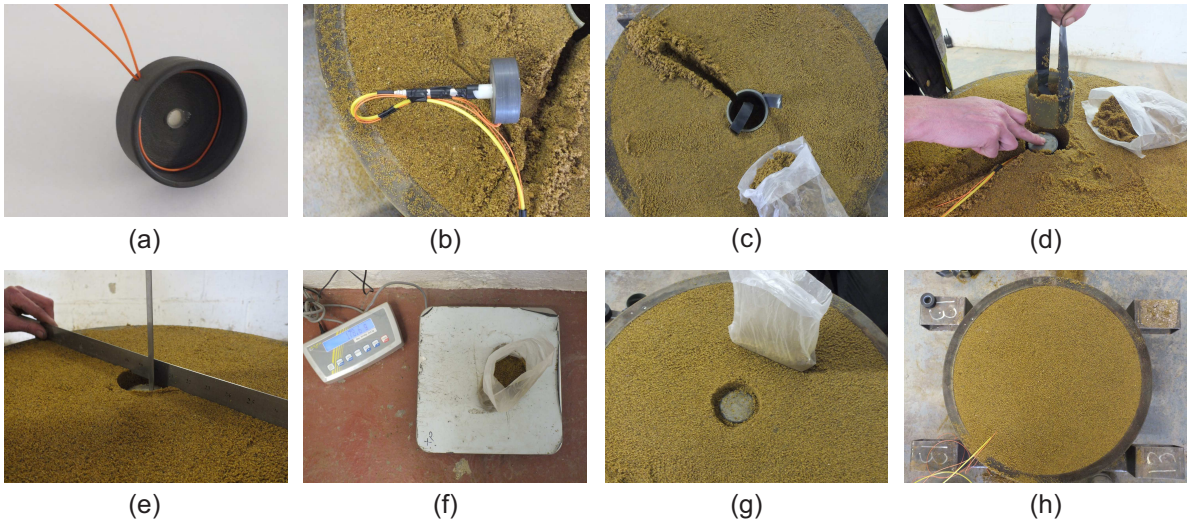

Figure 5: Images taken from charge preparation process: (a) charge case with breakwire, (b) non-el detonator and breakwire umbilical prepared for burial, (c) charge hole and umbilical trench prepared, (d) charge placement, (e) charge checked for depth and lateral alignment, (f) excavated material weighed, (g) overburden is placed, (h) container surface made good

Tests	Soil type	w (%)	ρ_d (Mg/m^3)	ρ (Mg/m^3)	Burial depth (mm)	Stand-off (mm)	W (g)	Explosive	Shape
1–5	Leighton Buzzard 14/25	2.50	1.60	1.64	28	140	78	PE4	3:1 cylinder
6–10	Leighton Buzzard 14/25	2.50	1.60	1.64	28	105	78	PE4	3:1 cylinder

Table 1: Summary of experimental test plan

4. Results and discussion

4.1. Example results at 140 mm stand-off

Figure 6 shows the pressure-time histories recorded at each bar location for Test 3, where the soil was located 140 mm beneath the target surface. The signals have been time shifted to remove the transit time of the elastic pulse between the loaded face of the HPB and the strain gauge location. The 0 mm bar is common for all HPB arrays and is included in each subplot. At this stage, the signals have not been corrected for Pochhammer-Chree dispersion [33]. The effect of dispersion for the current bar diameter and wave transit distance is a loss of definition of transient pressure features with durations <~5 microseconds, and the presence of spurious oscillations on the

pressure traces, but the general form of the pressure-time signals and the total impulse are unaffected. Figure 7 shows the specific impulse-time histories at each bar location for Test 3, where the specific impulse is given as the cumulative temporal integral of the pressure signal.

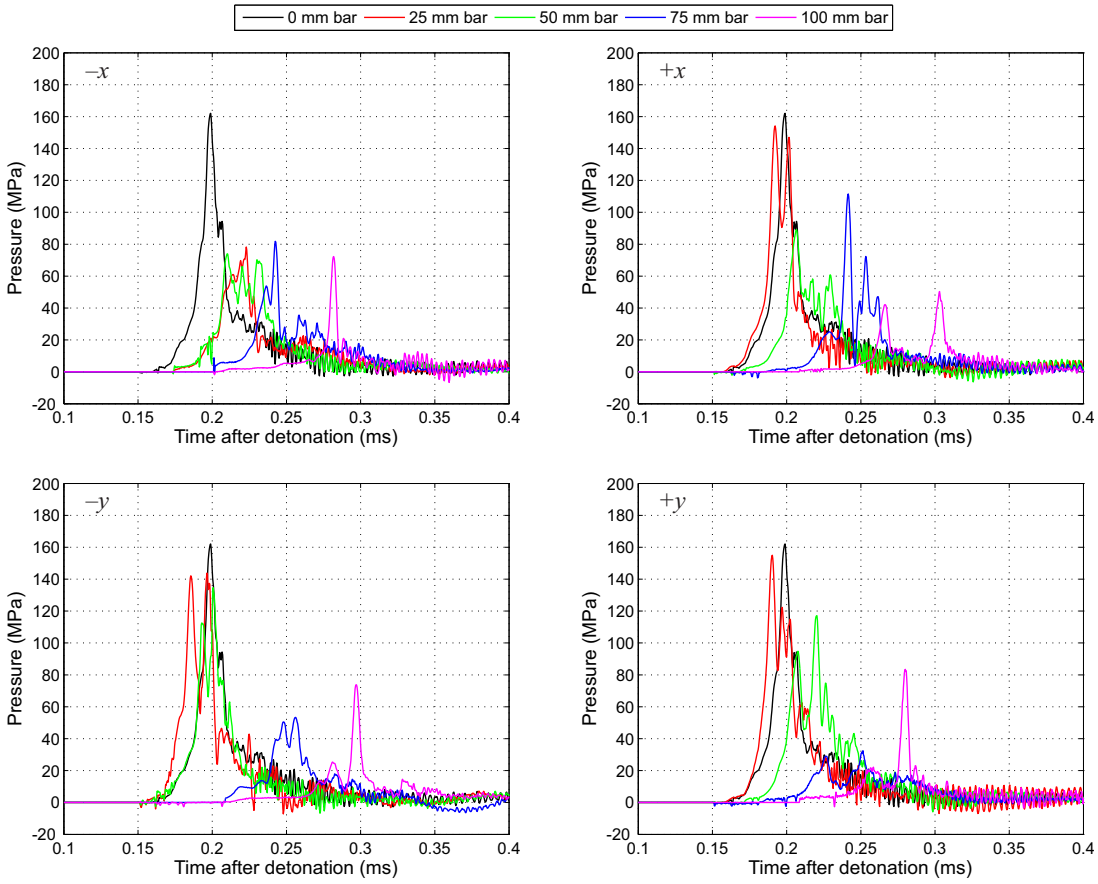

Figure 6: Example pressure-time histories for $-x$, $+x$, $-y$ and $+y$ arrays; Test 3 (140 mm stand-off)

A number of consistent features emerge from consideration of the pressure-time signals. The central bar exhibits a clear rise to peak pressure and a relatively uniform decay back down to ambient pressure thereafter. Further away from the target centre the behaviour differs, with multiple pressure spikes seen in the loading. This is perhaps most apparent in the 100 mm bar signals, and is best illustrated in the $+x$ array, where a clear rise to 42 MPa is seen at 0.27 ms after detonation, followed by a brief drop in pressure and subsequent rise to 50 MPa at 0.30 ms after detonation. This indicates that the mechanism of loading may differ as the expanding soil bubble/detonation

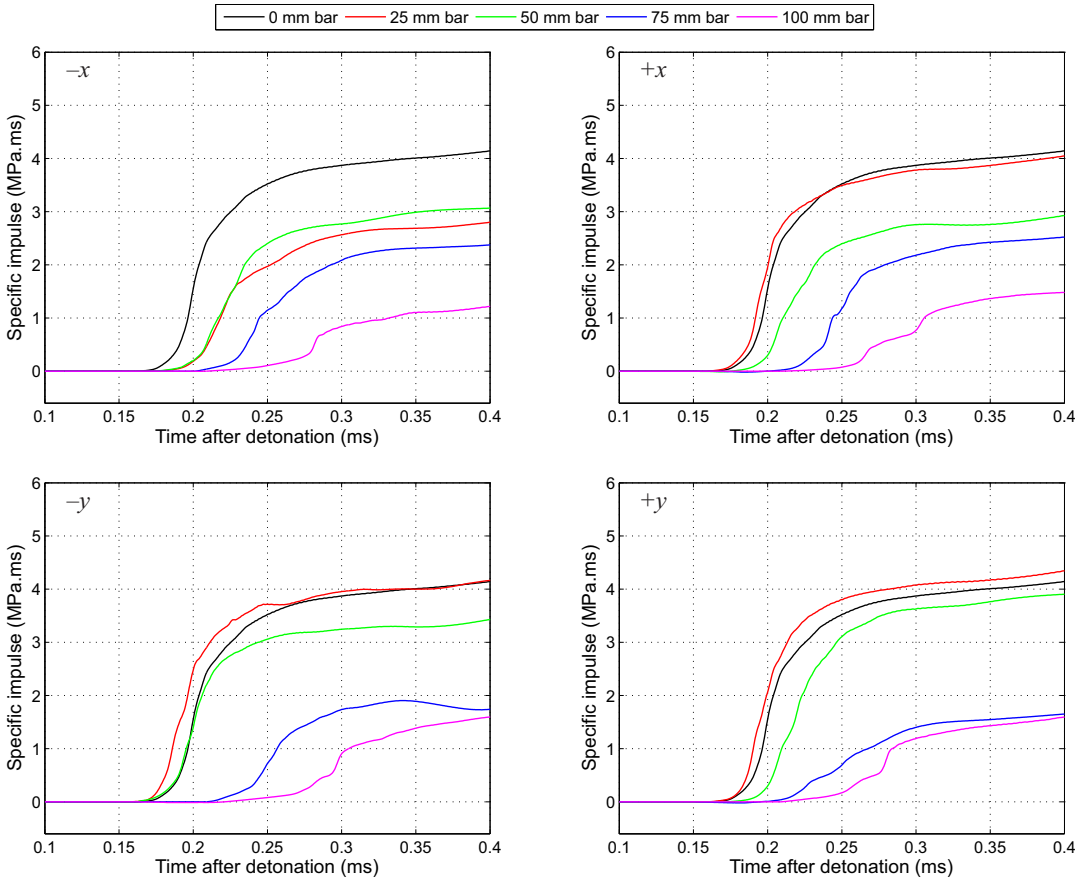

Figure 7: Example specific impulse-time histories for $-x$, $+x$, $-y$ and $+y$ arrays; Test 3 (140 mm stand-off)

product cloud propagates over the target face. Interestingly, the loading acts on the 25 mm bars in the $+x$ and $+y$ arrays and the 25 mm and 50 mm bars in the $-y$ array before acting on the central bar. This is indicative of non co-axial breakout of the soil and detonation products and emphasises the need for more than one HPB array for the current testing.

The specific impulse data is notably more consistent between tests, with the peak impulse for each bar generally appearing proportional to distance from the plate centre. Again, the clear multiple loading of the 100 mm bars can be seen with a 'step' like cumulative impulse profile (again the 100 mm bar in the $+x$ array shows this most clearly), whereas the more central bars exhibit a more regular cumulative increase in specific impulse.

4.2. Compiled results at 140 mm stand-off

Figures 8, 9 and 10 show the compiled peak pressure, peak impulse and time to peak pressure for each bar location for all five tests conducted at 140 mm stand-off. Time to peak pressure is presented as an alternative to arrival time as it is more clearly defined and less susceptible to sensor noise and the shape of the initial rise of the pressure pulse [19].

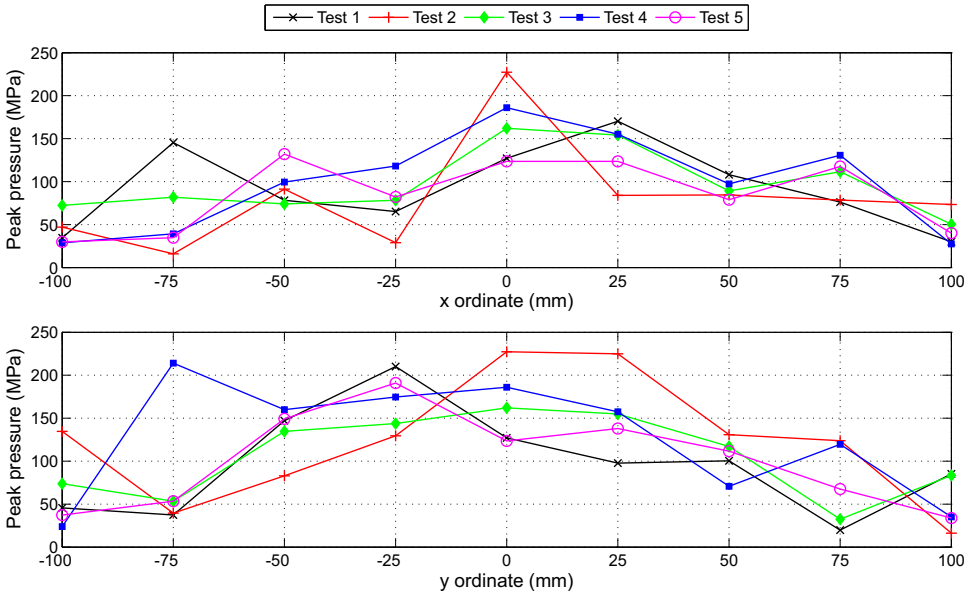

Figure 8: Compiled peak pressure; each bar location (140 mm stand-off)

Values of peak pressure vary between 227–124 MPa at the central bar and 135–16 MPa at 100 mm from the target centre. Values of peak specific impulse vary between 5.99–4.67 MPa.ms at the central bar and 2.58–0.89 MPa.ms at 100 mm from the target centre. This shows that there is a considerable decrease in the imparted load between the centre of the plate and a radial ordinate at only ~4 charge radii lateral distance from the target centre.

There appears to be a high degree of spread in the data: the maximum pressure in Test 4 is acting at the -75 mm *y* bar location; and the peak pressures in Test 2 appear to be skewed towards the +25 mm *y* bar location. Despite the apparent chaotic nature of the peak pressure recordings, the specific impulses and times to peak pressure appear more repeatable. However, the skewing of the data towards the +25 mm *y* bar location in Test 2 is also apparent

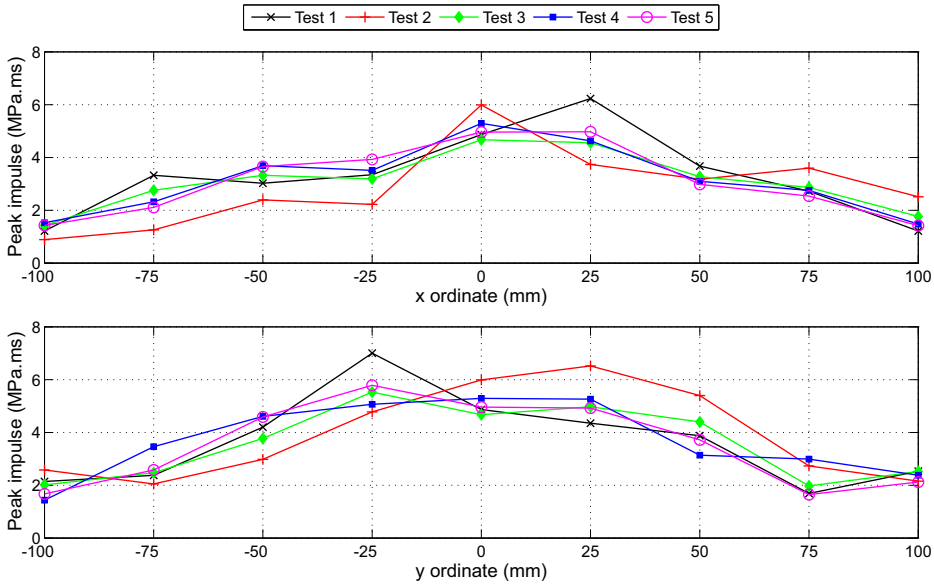

Figure 9: Compiled peak specific impulse; each bar location (140 mm stand-off)

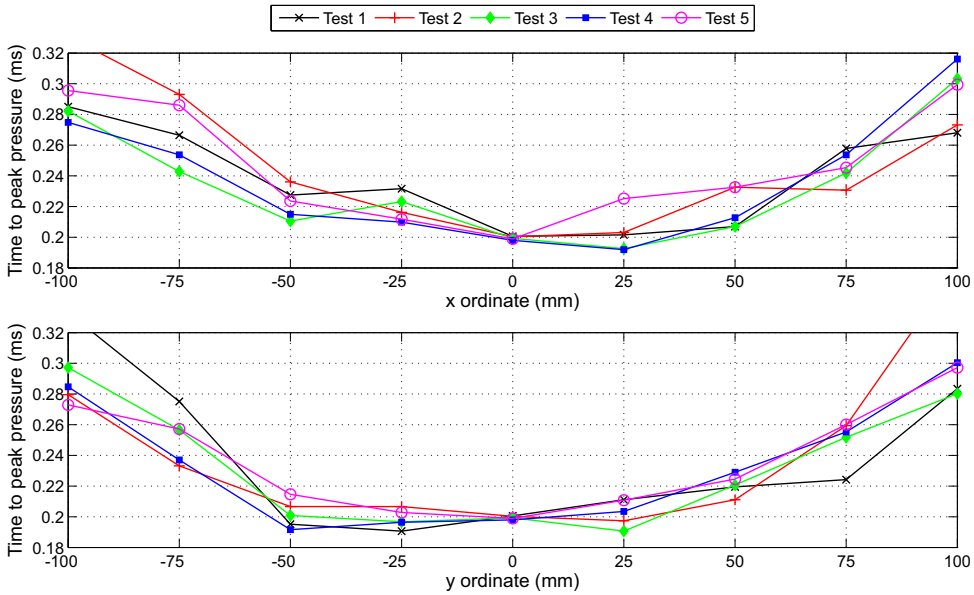

Figure 10: Compiled time to peak pressure; each bar location (140 mm stand-off)

in the impulse data. This bar lies almost directly above the charge periphery, and it is unlikely that such a feature could have been caused by non-central charge placement. Instead, it is likely that this is as a result of non-coaxial breakout of the soil bubble/detonation product cloud. This is justified by considering the time to peak pressure at this bar location. Here, the loading arrives some 3 μs earlier than the central bar, suggesting that this is indeed caused by non co-axial breakout as it is clearly recorded in the pressure, impulse and time to peak pressure test data.

Figure 11 shows the test-averaged compiled data for peak pressure, peak impulse and time to peak pressure. Here, the test-averaged value at each radial ordinate is given as the mean of the $-x$, $+x$, $-y$ and $+y$ values at that distance from the plate centre for that test, with the exception of the central bar where only one data set was recorded per test. Here, it can be seen that the variability has been substantially reduced. This agrees with previous observations that the global output from the explosive event remains relatively constant, whereas the localised loading is seemingly chaotic in nature [23].

4.3. Compiled results at 105 mm stand-off and comparison to 140 mm stand-off

The individual pressure-time and impulse-time histories at 105 mm stand-off do not differ significantly from the general form of the 140 mm stand-off tests. For brevity, individual test results are not shown in this section and only the test-averaged values are considered for further discussion (Figure 12). Figure 13 shows the effect of stand-off on loading parameters, where the mean values from each stand-off have been compiled and presented together for comparison. The total impulse to 100 mm radius has been calculated for each test by integrating the linear distribution of test-averaged impulse at each radial ordinate with respect to area.

It can be seen that the pressures and impulses are much higher magnitude for the reduced stand-off case. There is also a pronounced epicentral concentration of the pressure and impulse from the 105 mm stand-off tests with convergence of loading parameters with the 140 mm stand-off tests at higher radial offsets. There is a ~60% increase in the impulse over the central 100 mm radius as a result of the reduced stand-off.

4.4. Variability

A statistical analysis of the test data was performed. The mean values of peak pressure, peak impulse and time to peak pressure were evaluated for each bar location for tests 1–5 and tests 6–10 separately. This is the mean of 5 data points for the 0 mm bar and the mean of 20 data points for the 25–100 mm bars. The relative

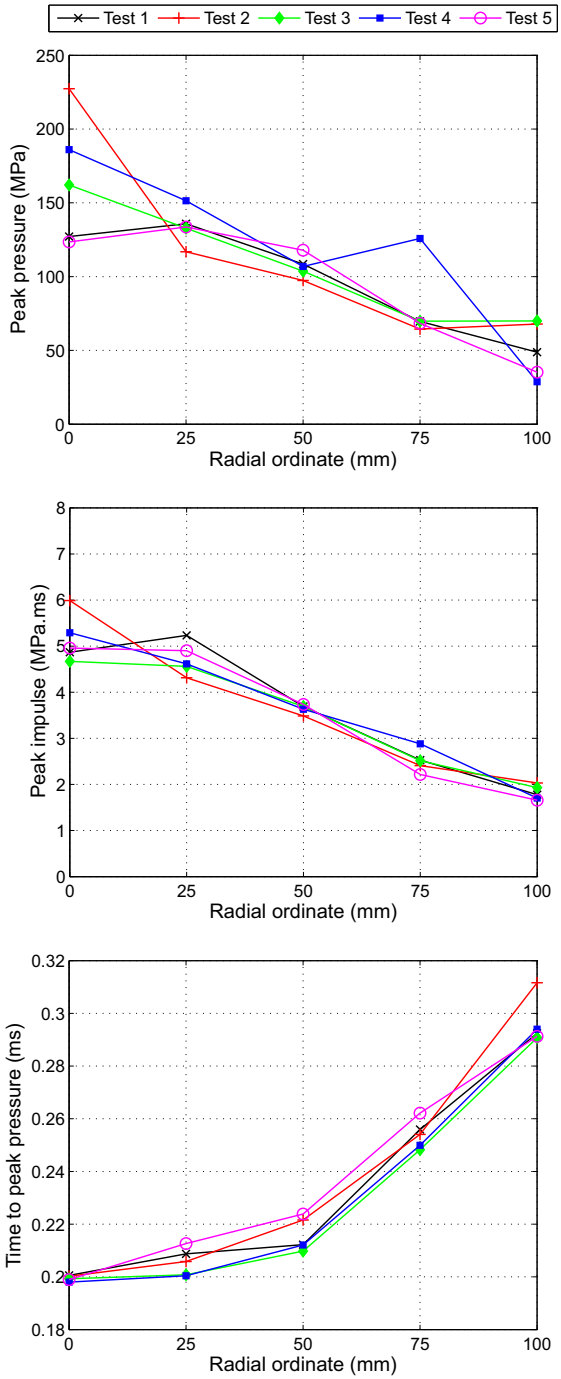

Figure 11: Compiled peak pressure, peak specific impulse and time to peak pressure; mean of $-x$, $+x$, $-y$ and $+y$ radial bar values for each test at 140 mm stand-off

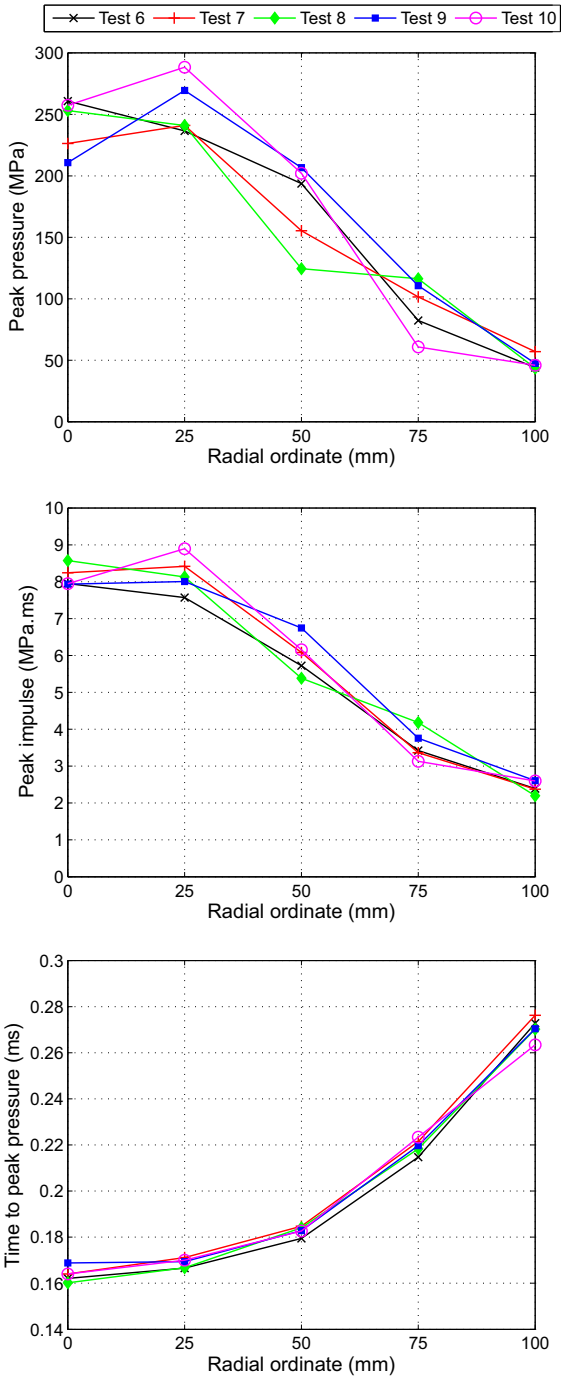

Figure 12: Compiled peak pressure, peak specific impulse and time to peak pressure; mean of $-x$, $+x$, $-y$ and $+y$ radial bar values for each test at 105 mm stand-off

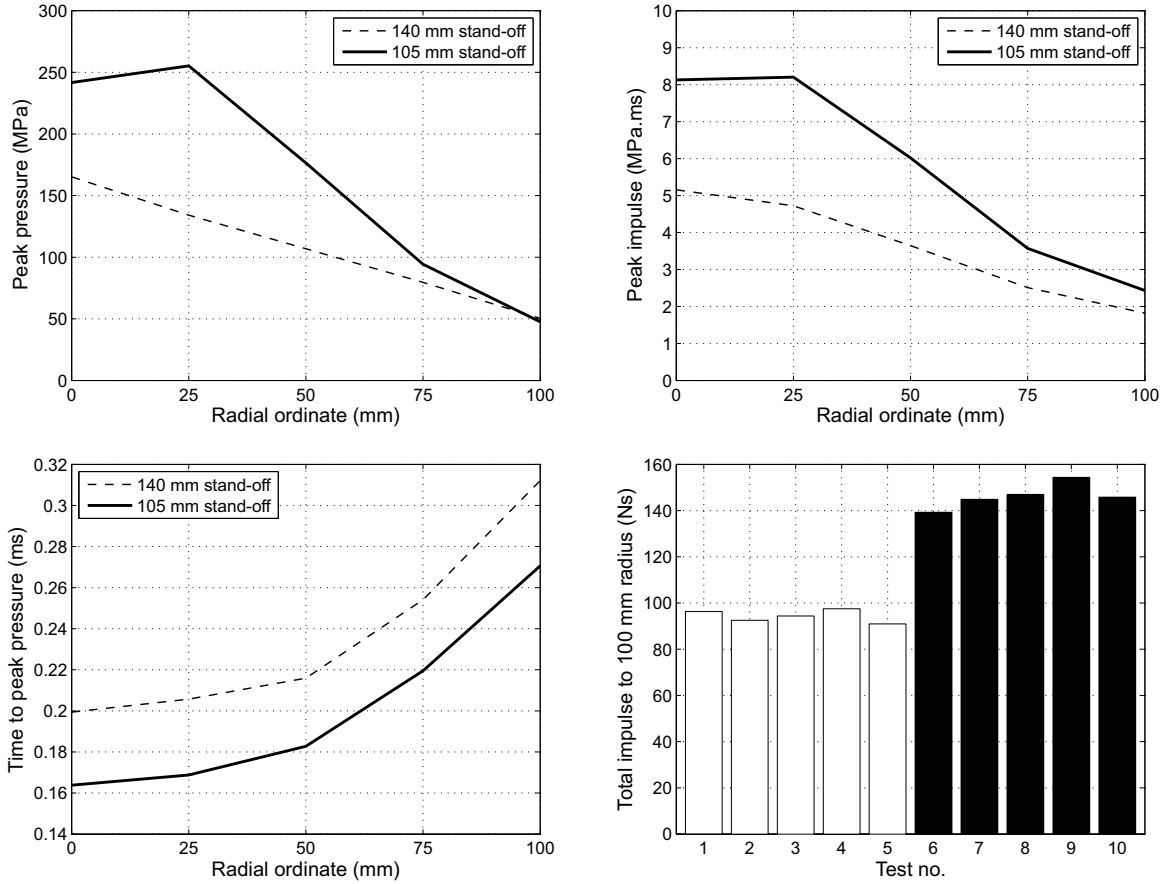

Figure 13: The effect of stand-off on loading parameters

standard deviation (RSD), given as the standard deviation divided by the mean, was also evaluated. Here, two values were calculated. The first value of RSD, 'per bar', is the RSD at each bar location considering each data point individually (as in Figures 8–10) and the second value of RSD, 'per test', is the RSD at each bar location considering the test-averaged data (as in Figure 11). Again, the 'per test' values for the 0 mm bar are identical to the 'per bar' values as only one data set was recorded per test. The statistical analysis is summarised in Table 2.

Variable	Stand-off (mm)	Bar location (mm)	Data points	Mean	Relative standard deviation (%)	
					Per bar	Per test
Peak pressure (MPa)	140	0	5	165.2	26.19	26.19
		25	20	134.1	37.49	9.145
		50	20	106.9	25.52	7.027
		75	20	79.62	64.07	32.59
		100	20	50.14	57.42	37.13
	105	0	5	241.7	9.101	9.101
		25	20	255.3	22.62	8.878
		50	20	176.5	27.50	20.08
		75	20	94.32	32.47	24.12
		100	20	47.60	37.21	11.48
Peak impulse (MPa.ms)	140	0	5	5.155	10.03	10.03
		25	20	4.725	25.13	7.457
		50	20	3.647	19.58	2.667
		75	20	2.510	24.23	9.634
		100	20	1.820	28.64	8.636
	105	0	5	8.129	3.439	3.439
		25	20	8.203	17.81	6.006
		50	20	6.018	14.17	8.476
		75	20	3.571	13.30	11.43
		100	20	2.432	11.15	7.101
Time to peak pressure (ms)	140	0	5	0.199	0.515	0.515
		25	20	0.206	5.766	2.543
		50	20	0.216	5.817	2.940
		75	20	0.254	6.850	2.157
		100	20	0.296	8.104	2.976
	105	0	5	0.164	1.961	1.961
		25	20	0.169	4.847	1.202
		50	20	0.183	6.126	1.116
		75	20	0.220	5.676	1.493
		100	20	0.271	4.527	1.734

Table 2: Statistical analysis of peak pressure, peak impulse and time to peak pressure. Relative standard deviation provided for all bar data ('per bar') and test average for each bar location ('per test')

The statistical analysis has confirmed that the test-to-test variance is considerably lower than the bar-to-bar

variance, with the RSDs decreasing considerably when taking the 'per test' values, typically by a factor between 2–7. This confirms the earlier observations that whilst the localised pressure and impulse measurements may be highly variable, the global output from the explosive remains relatively consistent. If the variability were intrinsically linked to the energetic output of explosive itself, for example, we should expect this variability to be present in the 'per-test' values also. As this isn't the case, we can conclude that the variability is predominantly caused by *localised spatial variations*.

The 'per test' RSDs of the time to peak pressure are all less than 3% of the mean. This suggests that the geometrical global expansion of the soil bubble is largely uniform and repeatable. The fact that peak pressures have the largest RSDs suggests that, within this uniform expanding bubble there are discrete regions of considerably higher pressure. This suggests that the apparatus may be capturing complex features such as jetting of the detonation products and differential momentum imparted to the soil within the expanding bubble. There is also a noticeable decrease in variability of peak pressure and peak impulse with decreasing stand-off distance. This shows that the localised high pressure/momentum instabilities also evolve temporally; the shorter the distance between the target and the soil surface, the less time these instabilities have to break away from the main soil bubble. This is consistent with findings from Taylor [21].

There is less than ±6% variation in total impulse for the two different test series when grouped by stand-off. Again, this shows that there is a good level of repeatability when considering global loading parameters.

The RSDs increase almost directly in accordance with distance from the plate centre, with this behaviour consistent for peak pressure, peak impulse and time to peak pressure. The cause of this will be explored in the section 5.

4.5. Comparison to previous work at the University of Maryland

In this subsection we compare our results to previous work conducted at the University of Maryland. Whilst the Maryland tests investigated the effect of stand-off, burial depth, and moisture content, only the most geometrically similar set of tests are used here for comparison. In these tests, 4.4 g Detasheet charges with diameter:height ratio of 3:1 were buried in dry sand, 10 mm below the soil surface, with the rigid target situated at a stand-off of 40 mm (section 5.4 in [22]). Assuming Detasheet (equal parts TNT and PETN) has the same TNT equivalence of PE4, the difference in scales between the Maryland and Sheffield tests is equal to $(78/4.4)^{1/3} = 2.61$. Therefore, at our scale, their tests equate to a 78 g PE4 charge buried at 26 mm with the target situated 104 mm above the soil surface,

enabling us to fairly compare this data to the results from our 105 mm stand-off tests. HPBs were placed up to an equivalent radial distance of 331 mm from the target centre, however only those results at positions equivalent to 0, 38, 66, 81, 102 and 133 mm are used for comparison in this section.

Figure 14 shows a comparison between the Sheffield and Maryland data, with the Maryland results scaled up to the same scale as the tests presented in this article. Peak pressure is independent of scaling, however specific impulse values require scaling by the cube-root of the relative charge masses, which is identical to the scale factor of 2.61 between the Maryland and Sheffield tests. Relative standard deviations are also shown for each bar location for peak pressure. Time to peak pressure data is not available in [22], nor are relative standard deviations for specific impulse and time to peak pressure. Test results from this article at 140 mm stand-off have been omitted to ensure a fair comparison.

The trends in both peak pressure and specific impulse with radial offset are similar, but the Maryland data are typically 20–30% higher for peak pressure outside the central region, and 15–20% higher for specific impulse. This could be as a result of increased directionality and focussing from the small-scale test setup. It is clear that the large-scale test data has a smaller peak pressure relative standard deviation than the small-scale test data, typically around half. This could be due to the control over preparation of the geotechnical test bed. We have previously demonstrated the importance of carefully controlling the geotechnical parameters in research concerned with the total impulse imparted to a target [32]. Alternatively, the difference could due to the differences in scaled particle size between the two data sets, resulting in more heterogeneous geotechnical conditions, and hence, more variable breakout of the detonation products from the soil cap in the smaller scale tests.

Furthermore, the Maryland tests used 6.35 mm diameter HPBs with the perimeter-mounted strain gauges placed at 305 mm from the loaded face. At our scale, this corresponds to 16.6 mm bars with strain gauges at ~800 mm from the loaded face. Accordingly we should expect Pochammer-Chree dispersion to be significantly larger in the smaller scale testing because of the relative increase in normalised frequency content and larger distance for the stress wave to propagate over. These potential issues have been minimised with the current arrangement detailed in this article.

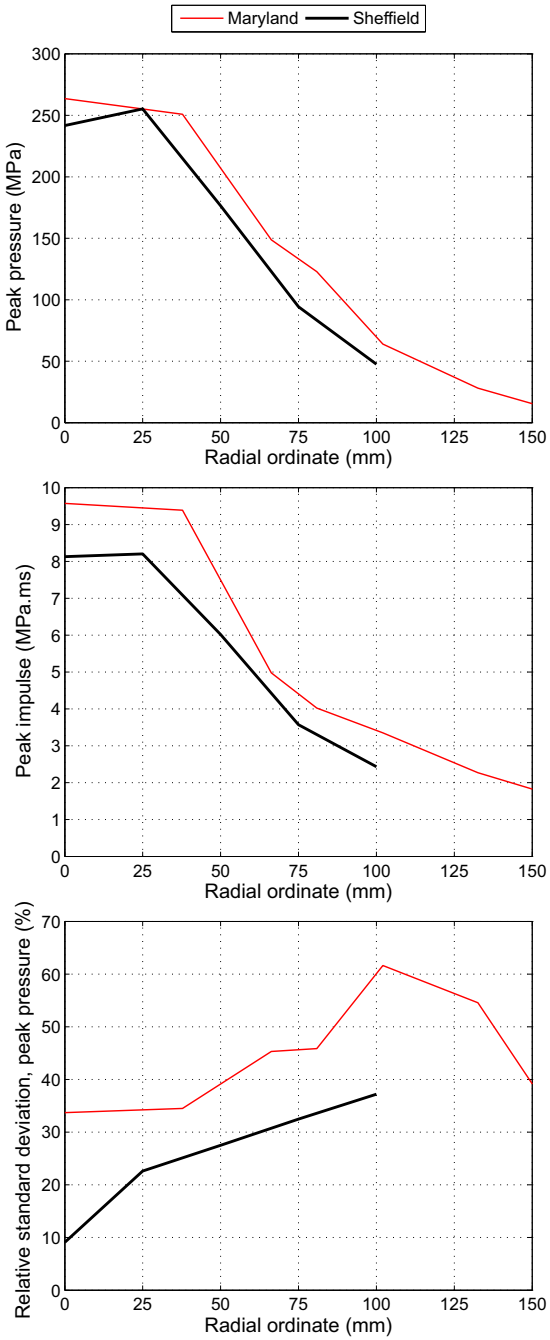

Figure 14: Comparison between previous work conducted at the University of Maryland (1/10 scale) and current data conducted at the University of Sheffield (1/4 scale)

5. Loading mechanism

5.1. Pre-impact

Figure 15 shows HSV stills of the early stages of soil bubble expansion from Test 5. As the first HSV frame corresponds to the moment of detonation, and we can observe the initial compressive stress wave reaching the soil surface in the third frame, at 0.03 ms after detonation, we can conclude that this stress pulse has travelled from the centre of the explosive to the soil surface at an average velocity of 1250 m/s. Spalling of the surface can be seen immediately upon arrival of the compressive wave at the soil/air interface. The soil bubble then rapidly expands, reaching a height of 57 mm above the soil surface at 0.10 ms after detonation, travelling at an average velocity of ~815 m/s. The soil bubble remains intact until approximately 0.14 ms after detonation, where partially reacted detonation products can be seen to vent into the surrounding atmosphere. The venting detonation products appear dark, suggesting that the overburden has quenched the combustion process and at this stage the reaction products *do not* react with the oxygen in the surrounding air.

As the soil is relatively dry, this rupture occurs at low values of volumetric expansion owing to a relatively low value of cohesive strength of the surrounding soil [26]. This early rupture gives rise to an increasingly non-uniform geometric expansion of the soil/detonation product mixture. Regions of jetting can be seen, where the expanding detonation products reach a preferential path through the surrounding soil skeleton. This also serves to focus localised areas of soil ejecta, and results in turbulent mixing at the interface between the products and the air, as suggested by Bergeron et al. [4]. As the soil/detonation product cloud is travelling at a supersonic velocity, it generates a pre-cursor shock wave which travels marginally in front of the head of the ejecta. This is difficult to discern from the HSV images presented in this paper alone, however it can be seen in the load data presented in the following subsection.

5.2. Loading phase

Figure 16 again shows HSV stills from Test 5, this time during the loading phase. Here the images are presented alongside plots of pressure distribution acting over a central 200 mm square region of the plate. The pressure distribution has been calculated from interpolation of the experimental HPB recordings from Test 5 using the algorithm outlined by Clarke et al. [2].

It can be seen at 0.20 ms after detonation that the very early stage of loading comprises several discrete particle strikes. These are roughly acting at the 25 mm bar locations in the $+x$ and $\pm y$ arrays, with a particularly large

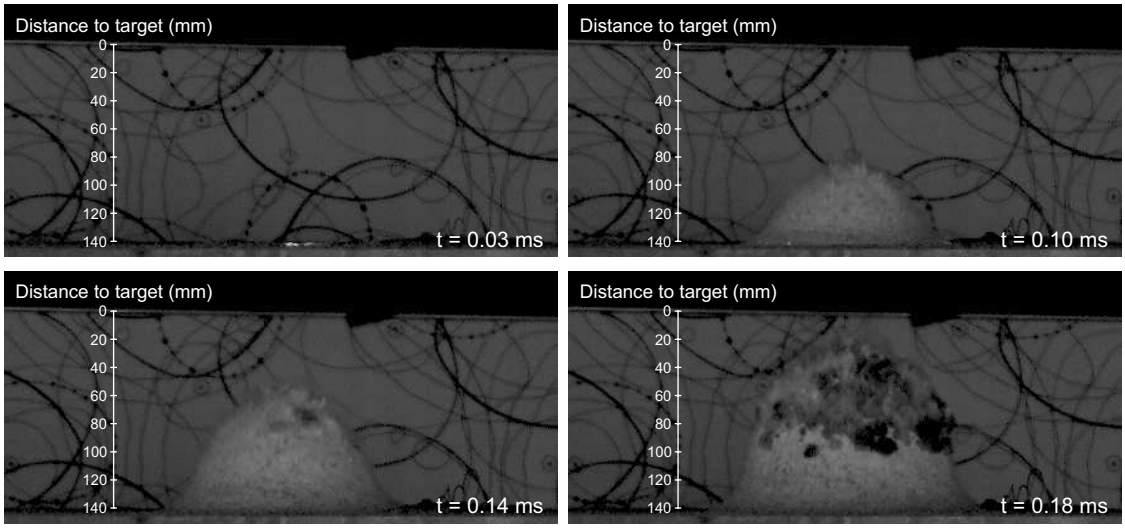

Figure 15: HSV stills showing early stage soil throw and breakout of detonation products; Test 5

magnitude strike (~200 MPa) occurring near the 25 mm bar location in the $-y$ array. These can be seen in the HSV stills as bright spots. This is either due to the impacting soil becoming incandescent as a result of the high velocity impact, or from localised re-ignition of the detonation products through combustion with the ambient air. The fact that these bright spots are visible up to 50 mm below the target surface suggests that it is in fact the latter, and therefore that some of the gases towards the centre of the bubble remain hot enough to react with the surrounding air once they begin to vent.

Alongside these discrete particle strikes, the pressure distribution shows a ~50 mm diameter region of relatively low magnitude (<30 MPa), uniform loading. This is caused by the the pre-cursor air shock [19], and can be seen quite clearly as the initial 'shoulder' in the 50 mm and 75 mm bar pressure-time histories from Test 3 in Figure 6.

At 0.21 ms after detonation the soil impact can be seen to loosely form an annulus of expanding material which propagates across the target surface. This has extended to a radius of approximately 40 mm from the target centre and can be seen as a flat, bright line at the interface between the soil/detonation product cloud and the underside of the target plate. Although still chaotic, the loading within this annulus appears to be gradually normalising as the hot gasses begin to equilibriate. The lateral expansion of the annulus and equilibriation of the material within the annulus continues for the next few tens of microseconds until a clear, well-defined annulus begins to form at 0.23 ms after detonation with a low-level, relatively spatially uniform load behind this expanding front. At this

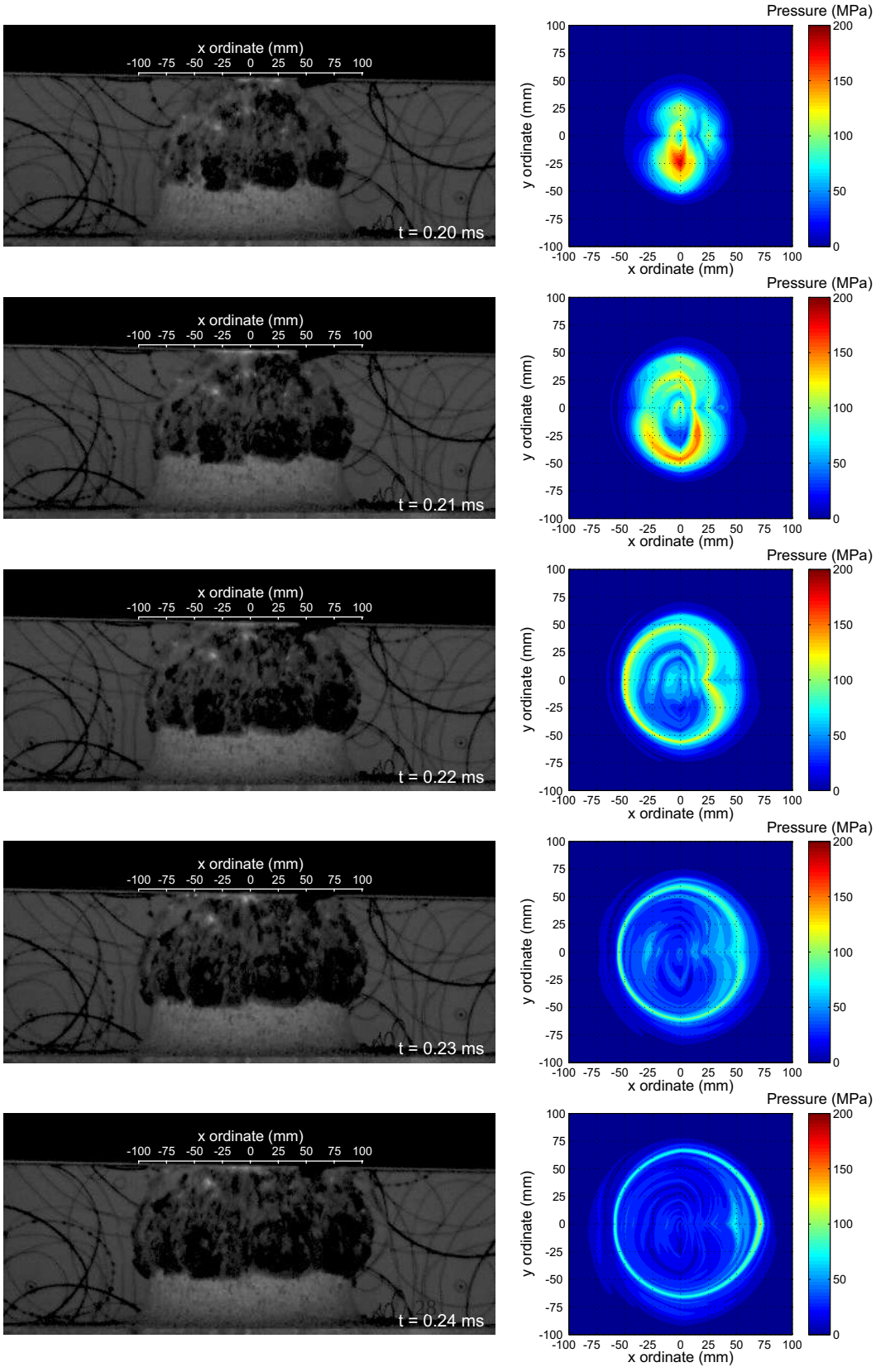

Figure 16: Synchronised HSV stills and interpolated pressure; Test 5

stage, the pre-cursor shock has reached a radius of some 75 mm from the target centre, with the soil annulus extending to 60 mm from the target centre. At 0.24 ms, the pre-cursor shock has almost reached the 100 mm bar location with the soil annulus lagging behind. The eventual detachment of the shock front from the ejecta cloud clearly explains the dual pressure spikes seen in the 100 mm bar pressure signals.

Whilst the early stages of loading appear the most chaotic from investigation of the HSV stills, it is worth remembering that the relative standard deviation of the recorded signals regularly *increased* with distance from the plate centre. It is clear, therefore, that the eventual pre-cursor shock detachment is intrinsically linked to the early-time chaotic breakout of the detonation products itself. Early breakout of the detonation products (directed along a given array) will result in a larger distance the unconfined products have to travel and higher energy losses through work done to the surrounding air. Delayed breakout of the detonation products gives rise to greater confinement, higher pressures, and the potential that the shock front may not detach in time and therefore superimpose with the expanding soil annulus. This explains the larger variability seen with increasing radial distance as reported in Section 4.4.

5.3. Late-time effects

After the main shock load there is a sustained particle barrage, which is fairly low magnitude and long duration (<10 MPa, ~1 ms). Whilst this loading is difficult to discern from the individual pressure-time histories, it becomes clear when considering specific impulse on an expanded *x*-axis, as in Figure 17. Here, the specific impulse is shown for the central bar from Test 6. Phase 2 loading, i.e. impact of the high-velocity detonation product and soil cloud, imparts around 75% of the total impulse, with the remaining 25% coming from the particle barrage in Phase 3 loading. There is a clear shoulder to the impulse-time history comprising the end of Phase 2 loading. The cause of this is presently unknown, but it provides clear evidence for the different mechanisms of Phase 2 and 3 loading.

6. Summary and conclusions

Direct measurement of the intense loading produced by the detonation of a buried explosive is an extremely difficult task. Historically, high-fidelity measurement techniques have not been sufficiently robust to capture the extremely high pressures associated with such events, and researchers have relied on ‘global’ measurements such as the average loading acting over a particular area of interest. Recently, an experimental apparatus has been

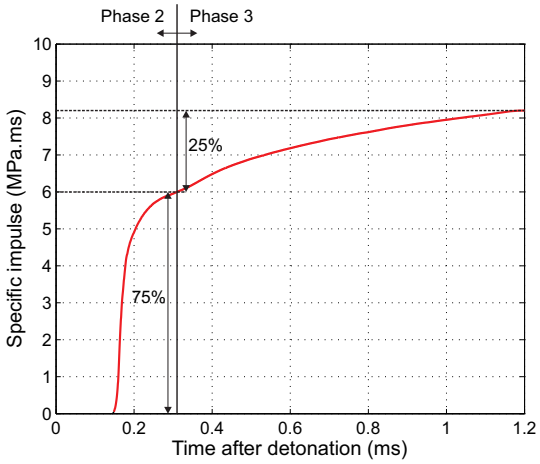

Figure 17: Specific impulse-time history at the central bar for Test 6 showing late-time contribution of Phase 3 to the total imparted impulse

developed by the current authors which provides temporally resolved pressure measurements at discrete points on a rigid reflecting surface [2].

This article presents results from ten experiments measuring the spatial pressure distribution from explosives buried in Leighton Buzzard (LB) sand. 78 g PE4 charges formed into a 57.1 mm diameter, 19 mm high cylinder were buried 28 mm beneath a soil surface which itself was located at stand-off distances of 105 mm and 140 mm from the underside of a rigid target. The LB sand was carefully prepared to achieve a moisture content of 2.5% and a bulk density of 1.64 Mg/m^3. Pressure was measured using 17 Hopkinson pressure bars within a radius of 100 mm from the centre of the plate. A high speed video camera, recording at 100,000 fps was used to film the event.

Individual pressure-time histories are presented for one test, and compiled peak pressure, peak impulse and time to peak pressure parameters are presented for both test series. For the 140 mm stand-off, peak pressure was shown to decay from a mean of 165 MPa at the central bar location to a mean of 50 MPa at the 100 mm bar location. The specific impulse demonstrated a similar trend, varying from a mean of 5.1 MPa.ms at the central bar location to a mean of 1.8 MPa.ms at the 100 mm bar location. For the 105 mm case, the peak pressure was considerably higher, decaying from a mean of 250 MPa in the central region to a mean of 47 MPa at the 100 mm bar location. The impulse decayed from a mean of 8.2 MPa.ms at the central bar location to a mean of 2.4 MPa.ms at the 100 mm bar location. In the 105 mm case, the values of maximum mean pressure and maximum mean

impulse were consistently seen at 25 mm from the target centre, rather than in the target centre as was the case with the 140 mm stand-off tests.

The pressure profile of the central bars appeared similar to a typical air shock, with more complex behaviour occurring at greater radial distances from the plate centre. Statistical analysis of the data indicated that pressure, impulse and time to peak pressure parameters increase in variability with distance from the plate centre. The variability was also seen to increase with increasing stand-off.

High speed video images were used in conjunction with recorded pressure data to examine the mechanism of loading from explosives buried in dry sand. It was found that the early stage of loading comprises chaotic soil ejecta/detonation product impact resulting in large, localised peaks in the applied loading. Following this initial impact stage, an annulus of ejected material begins to spread across the target face. At the same time, an air shock propagates ahead of the expanding soil/detonation product cloud and eventually detaches, causing the characteristic dual peak loading seen in the 100 mm bar pressure-time histories. Within the expanding annulus, the high pressure material begins to equilibriate and the spatial distribution of loading becomes more uniform. The main features of the load are complete tens of microseconds after detonation, with a low magnitude long duration particle barrage following, which comprises around 25% of the imparted impulse.

The results presented here have been compared with previous work conducted at significantly smaller length scales, but with similar sand particle sizes (hence, larger scaled particle size). The trends in peak pressure and impulse with scaled radial offset are broadly similar. However, the magnitudes appear both significantly higher and less consistent at smaller scale. This may be due to the relative effect of the detonator and the relatively coarse scaled particle size in the small scale tests. These results suggest that scale may be a significant issue in interpretation of experimental results.

Spatially and temporally resolved load measurements presented herein, as well as a detailed examination of the physical processes involved, enables a more rigorous validation of existing numerical approaches to be developed. This is of key importance to researchers and practitioners working in the field of buried explosives as it will in turn lead to better design of protective structures and the preservation of human lives.

7. Supplementary data

Full pressure-time histories for Test 3 (140 mm stand-off) and Test 8 (105 mm stand-off) are available to download with the online version of this article.

Acknowledgements

The authors wish to thank the Defence Science and Technology Laboratory for funding the published work, and technical staff at Blastech Ltd. for their assistance in conducting the experimental work reported herein.

[1] A. Ramasamy, S. D. Masouros, N. Newell, Adam M. Hill, W. G. Proud, K. A. Brown, A. M. J. Bull, and J. C. Clasper. In-vehicle extremity injuries from improvised explosive devices: current and future foci. *Philosophical Transactions of the Royal Society of London B: Biological Sciences*, 366(1562):160–170, 2011.

[2] S. D. Clarke, S. D. Fay, J. A. Warren, A. Tyas, S. E. Rigby, and I. Elgy. A large scale experimental approach to the measurement of spatially and temporally localised loading from the detonation of shallow-buried explosives. *Measurement Science and Technology*, 26:015001, 2015.

[3] B Hopkinson. A method of measuring the pressure produced in the detonation of high explosives or by the impact of bullets. *Philiosophical Transactions of the Royal Society of London. Series A, Containing Papers of a Mathematical or Physical Character*, 213(1914):437–456, 1914.

[4] D. Bergeron, R. Walker, and C. Coffey. Detonation of 100-gram anti-personnel mine surrogate charges in sand – a test case for computer code validation. Technical Report 668, Defence Research Establishment Suffield, Ralston, Alberta, Canada, 1998.

[5] M. Grujicic and B. Pandurangan. A combined multi-material Euler/Lagrange computational analysis of blast loading resulting from detonation of buried landmines. *Multidiscipline Modeling in Materials and Structures*, 4(2):105–124, 2008.

[6] A. B. Wenzel and E. D. Esparza. Measurement of pressures and impulses at close distance from explosive charges buried and in air. Technical report, U.S. Army Mobility Equipment Research and Development Center, Fort Belvoir, Virginia, USA, 1972.

[7] A. B. Wenzel and E. D. Esparza. The response of armor plates to landmines using model experiments. Technical report, U.S. Army Tank-Automotive Command (TACOM) Research and Development Center, Warren, Michigan, USA, 1974.

[8] P. S. Westine, B. L. Morris, P. A. Cox, and E. Z. Polch. Development of computer program for floor plate response from land mine explosions. Technical Report 13045, U.S. Army Tank-Automotive Command (TACOM) Research and Development Center, Warren, Michigan, USA, 1985.

[9] J. E. Tremblay. Impulse on blast deflectors from a landmine explosion. Technical Report DREV-TM-9814, Defence Research Establishment, Quebec, Canada, 1985.

[10] S. L. Hlady. Effect of soil parameters on landmine blast. In *Proceedings of the 18th International symposium on the military Aspects of Blast and Shock (MABS18), Bad Reichenhall, Germany*, 2004.

[11] M. Grujicic, B. Pandurangan, and B. A. Cheeseman. The effect of degree of saturation of sand on detonation phenomena associated with shallow-buried and ground-laid mines. *Shock and Vibration*, 12:1–21, 2008.

[12] S. D. Clarke, S. E. Rigby, S. D. Fay, A. Tyas, J. J. Reay, J. A. Warren, M. Gant, R. Livesey, and I. Elgy. 'bubble-type' vs 'shock-type' loading from buried explosives. In *Proceedings of the 16th International Symposium on Interaction of the Effects of Munitions with Structures (ISIEMS16), Florida, USA*, 2015.

[13] S Follett, A Hameed, S Darina, and J Hetherington. Numerical simulations as a reliable alternative for landmine explosion studies: the AUTODYN approach. In *Proceedings of the ASME 2010 International Mechanical Engineering Congress & Exposition, Vancouver, Canada*, pages 367–374, 2010.

[14] R.J. Moral, K. Danielson, and J.Q. Ehrgott Jr. Tactical wheeled vehicle survivability: Comparison of explosive-soil-air-structure simulations to experiments using the impulse measurement device. Technical Report ERDC/GSL TR-10-27, U.S. Army Corps of Engineers, Vicksburg, Mississippi, USA, 2010.

[15] T. Børvik, L. Olovsson, A.G. Hanssen, K.P. Dharmasena, H. Hansson, and H.N.G. Wadley. A discrete particle approach to simulate the combined effect of blast and sand impact loading of steel plates. *Journal of the Mechanics and Physics of Solids*, 59(5):940–958, 2011.

[16] D. M. Fox, X. Huang, D. Jung, W. L. Fourney, U. Leiste, and J. S. Lee. The response of small scale rigid targets to shallow buried explosive detonations. *International Journal of Impact Engineering*, 38:882–891, 2011.

[17] D.M. Fox, S.A. Akers, U.H. Leiste, W.L. Fourney, J.E. Windham, J.S. Lee, J.Q. Ehrgott, and L.C. Taylor. The effects of air filled voids and water content on the momentum transferred from a shallow buried explosive to a rigid target. *International Journal of Impact Engineering*, 69:182–193, 2014.

[18] W. L. Fourney, H. U. Leiste, A. Haunch, and D. Jung. Distribution of specific impulse on vehicles subjected to IED's. In *Proceedings of the IMPLAST 2010 Conference, Rhode Island, USA*, 2010.

[19] L. C. Taylor, W. L. Fourney, U. Leiste, and B. Cheeseman. Loading mechanisms from shallow buried explosives. In *Proceedings of the 24th International Symposium on Ballistics, New Orleans, USA*, 2008.

[20] W. L. Fourney, U. Leiste, and L. C. Taylor. Pressure irregularities in the loading of vehicles by buried mines. In *Proceedings of the 34th Annual Conference on Explosives and Blasting Technique, Cleveland, Ohio, USA*, 2008.

[21] L. C. Taylor, W. L. Fourney, and H. U. Leiste. Pressures on targets from buried explosions. *International Journal for Blasting & Fragmentation*, 4(3):165–192, 2010.

[22] H. U. Leiste. *Experimental studies to investigate pressure loading on target plates*. PhD thesis, Department of Mechanical Engineering, University of Maryland, USA, 2012.

[23] H. U. Leiste, W. L. Fourney, and T. Duff. Experimental studies to investigate pressure loading on target plates. *Blasting & Fragmentation*, 7(2):99–126, 2013.

[24] NATO. Procedures for evaluating the protection level of logistic and light armoured vehicles. *Allied engineering publication (AEP) 55*, Vol. 2 (for Mine Threat), 2006.

[25] A. Tyas, J. Warren, T. Bennett, and S. Fay. Prediction of clearing effects in far-field blast loading of finite targets. *Shock Waves*, 21(2):111–119, 2011.

[26] S. D. Clarke, S. D. Fay, J. A. Warren, A. Tyas, S. E. Rigby, J. J. Reay, R. Livesey, and I. Elgy. Predicting the role of geotechnical parameters on the output from shallow buried explosives. *Submitted for possible publication in International Journal of Impact Engineering*, –:–, 2016.

[27] S. D. Fay, S. D. Clarke, A. Tyas, J. Warren, S. Rigby, T. Bennett, I. Elgy, and M. Gant. Measuring the spatial and temporal pressure variation from buried charges. In *Proceedings of the 23rd International Symposium of Military Aspects of Blast and Shock (MABS23), Oxford, UK*, 2014.

[28] S. E. Rigby, A. Tyas, S. D. Clarke, S. D. Fay, J. Reay, J. A. Warren, I. Elgy, and M. Gant. Observations from preliminary experiments on spatial and temporal pressure measurements from near-field free air explosions. *International Journal of Protective Structures*, 6(2):175–190, 2015.

[29] A. Tyas, J. Reay, J. A. Warren, S. E. Rigby, S. D. Clarke, S. D. Fay, and D. J. Pope. Experimental studies of blast wave development and target loading from near-field spherical PETN explosive charges. In *Proceedings of the 16th International Symposium on Interaction of the Effects of Munitions with Structures (ISIEMS16), Florida, USA*, 2015.

[30] Barr AD. *Strain-rate effects in quartz sand*. PhD thesis, Department of Civil & Structural Engineering, University of Sheffield, UK, 2016.

[31] S. D. Clarke, S. D. Fay, A. Tyas, J. Warren, S. Rigby, I. Elgy, and R. Livesey. Repeatability of buried charge testing. In *Proceedings of the 23rd International Symposium on Aspects of Blast and Shock (MABS22), Oxford, UK*, 2014.

[32] S. D. Clarke, S. D. Fay, J. A. Warren, A. Tyas, S. E. Rigby, J. J. Reay, R. Livesey, and I. Elgy. Geotechnical causes for variations in output measured from shallow buried charges. *International Journal of Impact Engineering*, 86:274–283, 2015.

[33] A. Tyas and A. J. Watson. An investigation of frequency domain dispersion correction of pressure bar signals. *International Journal of Impact Engineering*, 25(1):87–101, 2001.